Optically Stimulated Luminescence (OSL) Dating in the Amazonian Wetlands

Optically Stimulated Luminescence (OSL) Dating in the Amazonian Wetlands

Edited by

Sonia Hatsue Tatumi,
Dilce de Fátima Rossetti and
Emílio Alberto Amaral Soares

Cambridge
Scholars
Publishing

Optically Stimulated Luminescence (OSL) Dating
in the Amazonian Wetlands

Edited by Sonia Hatsue Tatumi, Dilce de Fátima Rossetti
and Emílio Alberto Amaral Soares

This book first published 2020

Cambridge Scholars Publishing

Lady Stephenson Library, Newcastle upon Tyne, NE6 2PA, UK

British Library Cataloguing in Publication Data
A catalogue record for this book is available from the British Library

ISBN (10): 1-5275-5430-9
ISBN (13): 978-1-5275-5430-6

TABLE OF CONTENTS

PREFACE

Ages evaluated by optically stimulated luminescence (OSL) dating proved to be extremely useful in establishing the late Quaternary chronological framework of many areas in the Brazilian territory. This is due to the generally low potential of sedimentary organic matter preservation, which is particularly critical in the Amazonian wetlands areas because of the hot weather and high precipitation rates. On the other hand, the fluvial and aeolian sedimentary successions of quartzose sand sediments prevailing over this region are suitable for dating by OSL. More than twenty years of continuous and collaborative work resulted in an extensive database of OSL ages for the Amazonian late Quaternary sedimentary deposits. This effort has contributed to improving the paleoenvironmental and paleoclimatic reconstructions of this region within this period. This book has the main goal of providing the state of art on the OSL dating of late Quaternary deposits in the Amazonian wetlands. Chapter 1 contains an introduction to the OSL method and its use in sediment dating. The theory of point defects in the crystal lattice is described, as well as the kinetics of OSL emission. This chapter also addresses the OSL responses of different types of quartz found in Brazilian sediments, and some problems found in OSL response of pink and hyaline quartz. The methodology used to determine the age of sediment deposition with the assessment of the equivalent dose and annual dose rate is also explained. Chapter 2 provides an overview of the geological framework of the Amazonian wetlands, with particular emphasis on the lithological characteristics description and the Quaternary sediments depositional environments. Main scientific questions focusing on the Quaternary period in this region are raised to highlight the need of improving the OSL chronology. In chapter 3, we discussed the main problems faced when dating Quaternary sediments from the Amazonian wetlands. Methodological approaches, including results of the SAR protocol and age models applied to some sediment samples from this region, are also included in this chapter. Chapter 4 contains a summary of OSL ages available for Quaternary sediments of terraces from various Amazonian rivers. Also included are OSL ages of sediments formed by distributary rivers in megafan systems or aeolian processes, as these types of sediments represent a significant proportion of the Quaternary

sedimentary record. We end this book commenting on future developments planned to be applied for improving the OSL dating technique of the Amazonian Quaternary sediments.

PROLOGUE

This book summarizes the interdisciplinary investigation undertaken by a pioneering team of physicists and geologists, who have been interacting scientifically for the past two decades to establish the OSL chronology of Quaternary sediments from the Amazonian lowlands. The application of this dating technique proved to be valuable for addressing several scientific issues concerning the Quaternary history of this region, mainly including depositional environments, changes in vegetation patterns, climatic variations and paleoseismicity due to tectonic reactivations. The group began the dating research in Amazonia using the Thermoluminescence (TL) and OSL methods (Tatumi et al., 2002; Carneiro Filho et al., 2002), following the multi-aliquot regenerative-dose (MAR) protocol (Murray and Mejdahl, 1999, Hilgers, et al., 2001) for the determination of dose equivalent (D_e). Due to the variation in the OSL response of each aliquot, the natural normalization (NN) process was implemented to determine the sensitivity of each aliquot (Rhodes and Pownall, 1994). This procedure was obtained by the OSL response of the aliquots to the short exposure to the stimulating light, which helped subsequent corrections. However, this light exposure could decrease the sample age, which was particularly troublesome when dating young samples. For this reason, to date young and dimmer samples, we have adopted the Dose normalization (DN) after the end of the measurements used for D_e evaluation, with the OSL intensities of the aliquots being measured after irradiation with the same standard dose. The disadvantage of this procedure was the response variation to previous procedures, such as preheating, irradiation and bleaching.

The dose normalization was no longer required with the development of the single aliquot method (Duller, 1991). Although the normalization resulting from natural variations in the OSL responses of each aliquot was removed, response fluctuations of the aliquots from OSL growth curve procedures remained. To address this problem, Murray and Roberts (1998) suggested using the single aliquot regenerative dose (SAR) protocol, where the OSL measurement of each natural or regenerated dose is corrected for changes in sensitivity using the OSL response obtained after previous constant test dose. Recycling, recuperation and dose recovery tests were suggested as complements of the SAR protocol (Murray and

Wintle, 2000), which was adopted by our team. Previous dating results obtained by the MAR protocol were then repeated by using also the SAR technique, and this comparative work was documented elsewhere (e.g., Soares et al. 2010, Gonçalves Jr. et al. 2016, Sant'Anna et al., 2018). Increased age accuracy was observed using the SAR protocol, as well as the Central Age, Minimum Age and Finite Mixture age models (Galbraith et al., 1999, Galbraith and Roberts, 2012), especially when dating river sediments, which prevail in the Amazonian lowlands. Despite the already available advanced results of OSL dating, further efforts are still needed to achieve a robust chronostratigraphic framework for the Quaternary sediments of this region. This type of information is crucial to help investigations aiming to unravel the Quaternary history of Amazonian rivers.

CHAPTER ONE

OPTICALLY STIMULATED LUMINESCENCE

1.1 Introduction

The dating method of applying optically stimulated luminescence (OSL) was initiated in the mid-1980s under the name "Optical Dating", the green light emitted by an argon laser was used to excite quartz grains and ages were determined successfully (Huntley et al., 1985). Since then, the number of publications that have used OSL dating techniques to help reconstruct the Quaternary depositional history of various regions over the world increased considerably (e.g., Moska et al., 2011; Lyons et al., 2014; Dogan et al., 2015; Portenga and Bishop, 2015; Hardt et al., 2016; Cunha et al., 2017; Gilles et al., 2017, Larkin et al., 2017; Long et al., 2017; Cawthra et al., 2018; Wang et al., 2018).

The OSL method is based on the fact that when grains of sediments are exposed to sunlight, they release charges previously accumulated by ionizing radiation in the grain structure (Prescott and Robertson, 1977). The trapped charges result from damages caused by the interaction of the mineral with alpha and beta particles, as well as gamma radiation. These particles are derived from cosmic rays and the disintegration of naturally occurring radioactive isotopes, such as ^{235}U, ^{238}U, ^{232}Th and ^{40}K, present in or near minerals. Radiation bleaching occurs in the depositional environment when sediments are exposed to sunlight (Aitken, 1985; Duller, 2004). If exposure is sufficient to remove any preexisting signal, absolute ages for the depositional time can be determined based on estimates of the time elapsed since the last exposure of sediment grains to daylight and the rate of renewed radiation accumulated on the grain surface after burial.

Major advances in technologies and protocols for the measurement of the ionizing radiation of sediment grains has occurred in the last years. Among these, the development of dating techniques based on OSL represented an improvement over the thermoluminescence method, because of: the ability to date sediments exposed to daylight for a short period of time, which increased the dating of samples from a variety of

environments where sediment transport and deposition occurred subaqueously; and the decrease in the degree of uncertainty for which the luminescence signal is zeroed, which allowed the precise dating of young samples deposited even in the last few centuries (Duller, 2004).

Another advancement of OSL dating was the ability to estimate ionizing radiation accumulated on quartz grains (Duller, 2004). The date of this mineral is preferred to the previously used feldspar grains because the latter proved to provide underestimated luminescence ages (Wallinga et al., 2001). In addition, quartz luminescence can be readily stimulated using automated, highly sensitive and reproducible luminescence systems based on low-cost LED light sources (Bottler-Jensen et al., 1999). The development of the *single-aliquot regenerative-dose* (SAR) protocol (Murray and Wintle, 2000) also contributed to increasing the accuracy of luminescence measurements, as well as to reducing costs and time of analysis.

1.2 The OSL theory

1.2.1 Principles

OSL is defined as the light emitted by some crystals previously irradiated with ionizing radiation when stimulated by light in the visible or infrared region. The OSL of quartz crystals can be stimulated with blue or green light, with the luminescence detected in the ultraviolet (UV) region. Similarly, feldspar crystals have their luminescence detected in the UV region, however, the stimulation is done with infrared light. In both cases, the OSL can be characterized as an anti-Stokes emission. The excitation of quartz with blue light (440 – 485 nm) is generally more effective than with the green light (500 – 565 nm) originally used by Huntley (1985). The name OSL refers to the technique applied when using blue or green light to stimulate quartz grains, and Infrared Stimulated Luminescence (IRSL) when using these lights to stimulate feldspar grains.

OSL emission of natural crystals is not yet fully understood because it depends on the nature and concentration of impurities, as well as on defects contained in the crystal. Because each mineral may have different OSL response, even aliquots of the same sample must be calibrated individually. It is well known that crystals in nature are not perfect. Thermodynamic imperfections are created in the crystal lattice, causing ions to move from their normal positions and locate either in interstitial positions or on the surface of the crystal. Mott and Gurney (1940) showed that the concentration of these defects (n_d) increases according to the equation:

$$n_d = e^{-\frac{W}{2kT}} \tag{1.1}$$

where W is the work required to move an ion from its position in the crystalline lattice; T is the absolute temperature; and k is the Boltzmann constant. In addition to defects, crystals may have impurities, such as ions that are not part of their original crystalline lattice.

The main defects that can be found in a crystal are shown in Fig.1.1. In this figure, vacancies and interstitial defects, i.e., ions displaced from their original positions, are considered intrinsic defects. Pair of vacancy - interstitial ion forms the Frenkel defect, and pair of cation - anion vacancies creates the Schottky defect. F-center is an anion vacancy filled by an electron. The extrinsic defect is created when an impurity, such as Fe, Al, Ti and Li, can assume the position of an original ion site in the lattice or interstitial position at the time of crystal formation. All these defects are commonly referred to as point defects.

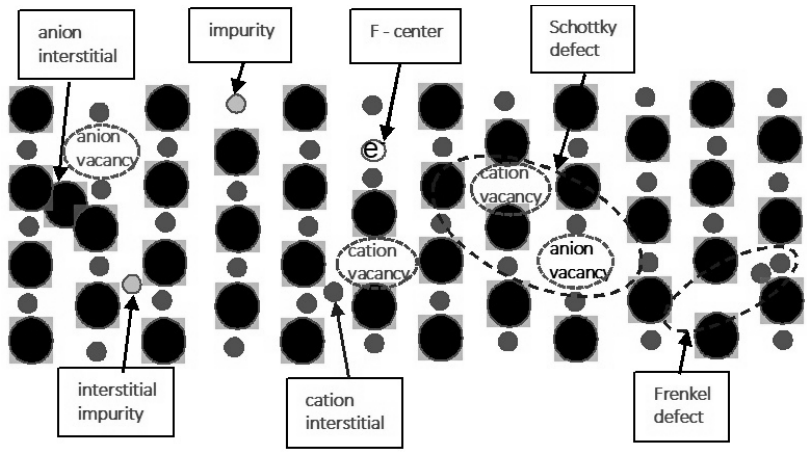

Figure 1.1: Examples of points defects in ionic crystals (F-centre is an anion vacancy filled by an electron).

Using energy band models, the point defects of crystals are in the forbidden band (FB). When a crystal is irradiated with ionizing radiation, part of its energy is transferred to the charges in the valence band (VB). As a result, some electrons receive enough energy to jump at the conduction band (CB). Later, the electrons can be trapped in electron traps located in the FB, forming metastable levels. Similarly, metastable levels occur with trapped holes, characterized by activation energy *(E)* and frequency factor*(s)*. *E*

characterizes the depth of the trap. Crystals might have traps with different *E* values, which define a trap as shallow or deep. The parameter *s* is the vibration frequency of the trap. Electrons remain trapped for microseconds to millions of years (depending on the energy level of the trap), so the mean life (τ) of the metastable levels can be calculated by:

$$\tau = \frac{exp\left[\frac{E}{kT}\right]}{s} \tag{1.2}$$

When OSL measurements are performed, the crystals are optically stimulated, which releases electrons from the traps and moves them to the CB, so that they can be re-trapped or recombined with trapped holes in the recombination center.

1.2.2 Band model applied to quartz OSL

The band model is generally used to explain the OSL emission (McKeever and Chen, 1997; Bailey, 2001). A model developed by Bailey (2001; Fig.1.2A) is specifically applied for natural quartz, which is the mineral most commonly used in sediment dating. Five electron traps, denoted by i=1 to 5, are used to explain the dating process. In the scheme of Fig.1.2A, i=1 and 2 are related to Thermoluminescence (TL) emission of 110 ºC and 230 ºC peaks, respectively. The 110 ºC TL peak is light sensitive and can exhibit phototransference during the emission of the OSL fast component. The traps i=3 and 4 are related to the OSL emission of fast and medium components, and the level i=5 represents an optically insensitive trap. The shallow centers of the holes are denoted by j=6 and 7, which are thermally unstable and can be a luminescence center or killer center. The trap j=8 is the L-center, where the electron from the CB can recombine with trapped holes and emit luminescence. The trap j=9 is a thermally stable killer center and competes with the electrons from the CB. Bailey (2004) added levels 5, 6, and 7 (Fig. 1.2B) to represent slow OSL components (named S1, S2, and S3). In addition, levels 10 and 11 were introduced by Pagonis et al. (2008) to relate source traps for the TT-OSL and BT-OSL signals (Fig. 1.2C). OSL studies have also indicated several slow components (Jain et al, 2003; Singarayer and Bailey, 2003).

Previous studies on OSL emission revealed that, when an electron and hole recombination occurs, the luminescence center becomes excited, resulting in the OSL emission and relaxation of the luminescence center to the ground state (Ankjærgaard and Jain, 2010).

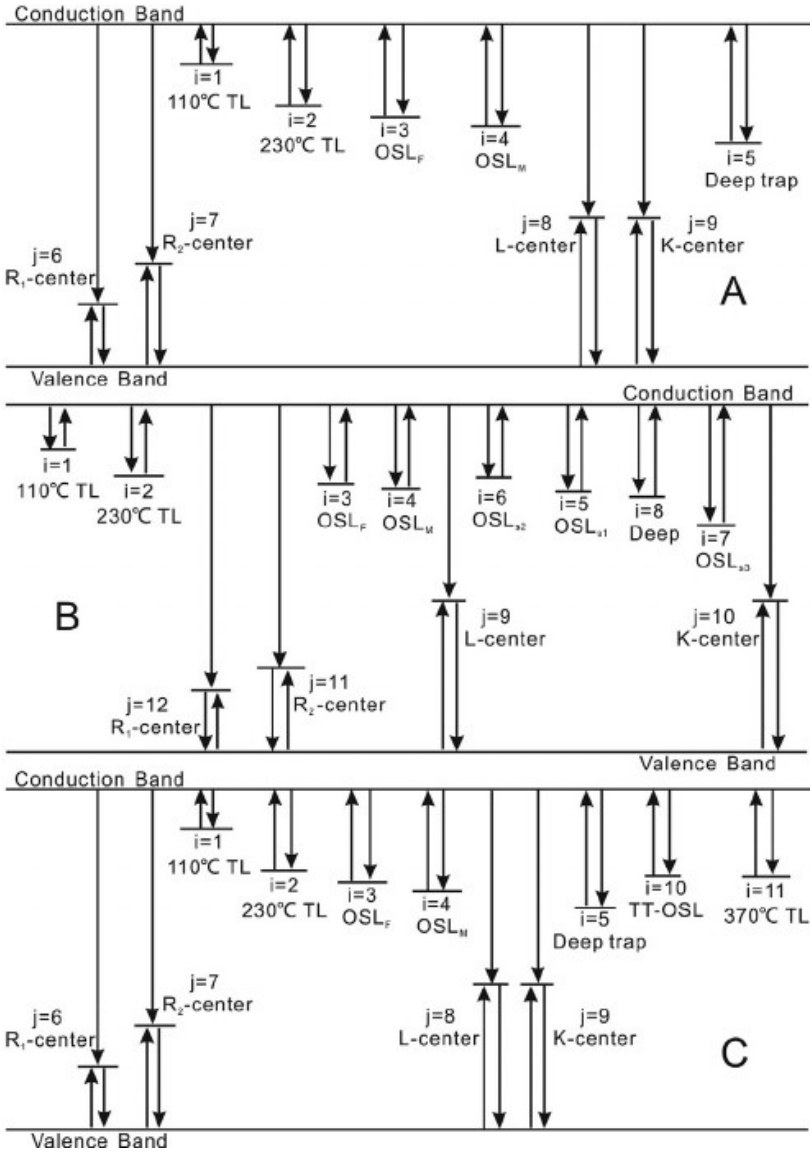

Figure 1.2. Schematic diagrams of the comprehensive quartz models according to: A) Bailey (2001). B) Bailey (2004). C) Pagonis et al. (2008). Adapted from Peng and Pagonis (2016).

1.2.3 OSL application in dating

In principle, the OSL intensity is proportional to the amount of the dose (D_e = *[J / kg = Gy]*) accumulated in the crystal by the ionizing radiation, which in turn is proportional to the exposure time or age of the sample to this radiation. The age for coarse-grain sediments (~100 μm) is calculated according to the equation:

$$Age = \frac{D_e}{0.90D_\beta + D_\gamma + D_C} \tag{1.3}$$

Where D_e is the equivalent dose, i.e., the accumulated dose in the crystal; D_β is the annual dose rate provided by beta particles; D_γ is the gamma radiation rate; and D_C is the contribution or rate of cosmic rays. The beta particle and gamma radiation came from the natural radioisotopes in soils, mainly U, Th (as well as their radioactive daughters) and K-40. The numerical factor 0.90 is due to the attenuation of the beta contribution (Aitken, 1998). These rates should be corrected taking into account the water content to obtain wet dose rates, which are given by:

$$D_\beta = \frac{D_{\beta dry}}{1+1.25WF} \tag{1.4}$$

$$D_\gamma = \frac{D_{\gamma dry}}{1+1.14WF} \tag{1.5}$$

Where, W is the saturation water content (water weight / dry sediment weight), and F is the saturation fraction related to the average water content assumed over the entire burial period. The contribution of cosmic radiation is theoretically calculated by knowing the geographical coordinate values of the sampling site, following the equation of Prescott and Stephan (1982).

A new protocol summarizing all the improvements of the OSL method during the 1990s was provided by Aitken (1998). The OSL signal can vary greatly from aliquot to aliquot, resulting in a very large margin of error, especially in young (Holocene) fluvial sediment samples, due to the different sunlight bleaching of each grain in an aliquot.

The OSL response is extremely sensitive to the preheating temperature used to eliminate the contributions from unstable or metastable centers. The OSL signal also presents the phototransfer phenomenon, which occurs when electrons are released to the CB by illumination. In this case, the electrons may be retrapped in traps related to the 110 ºC TL peak. We

observed phototransfer phenomena in hyaline and pink quartz grains in Brazil (Tudela, 2018). These are almost pure quartz crystals, with only a few traces of impurities. Fig. 1.3 shows an intense phototransfer phenomenon in CW-OSL measurements of aliquots of a hyaline quartz grain preheated to 160-240 °C (Fig.1.3A-C). However, this phenomenon was not observed at temperatures higher than 240-260 °C (Fig.1.3D, E). The reference background (BG) level for measurements at 240 ºC is still high and stabilized only after 260 ºC.

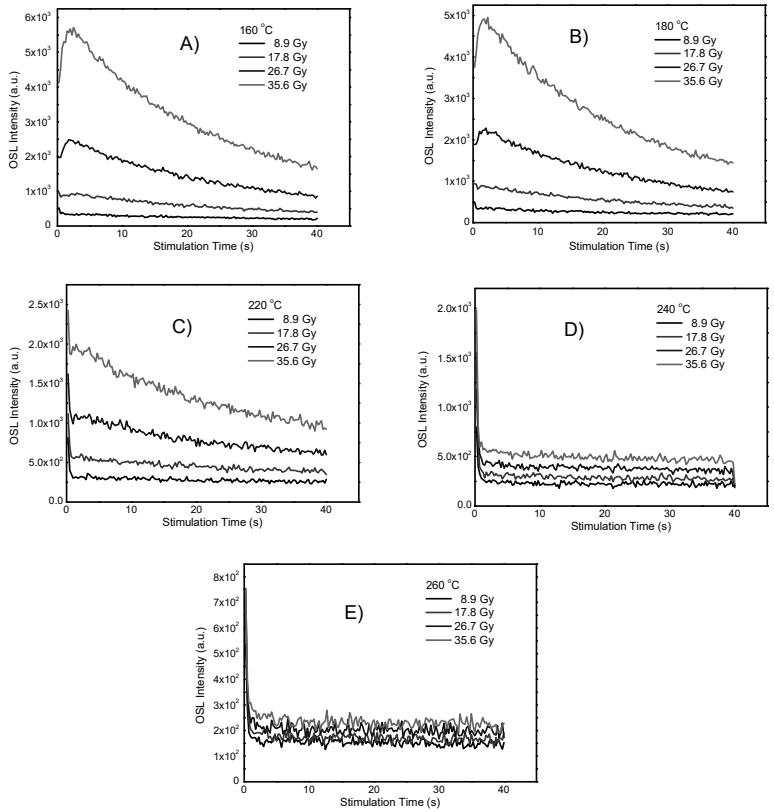

Figure 1.3. CW-OSL curves of hyaline quartz obtained after irradiation with different beta doses and preheating. A) 160 °C. B) 180 °C. C) 220 °C. D) 240 °C. E) 260 °C. (Tudela, 2018).

To verify the origin of phototransfer traps, bleaching experiments were performed, with residual TL glow curves being obtained with aliquots subjected to irradiation cycles using blue light (470 nm) illumination from 0.5 to 700 s and TL measurements (Tudela, 2018).

Fig. 1.4 shows the results obtained for TL measurements detected in the UV region. Two TL peaks at a temperature below 220 ºC were observed, one at 134 °C and the other at 187 ºC. The peak intensities in both cases increase up to 5 s of illumination, and then they decrease. After 150 s, almost all the entire TL signals reached a constant value. In this case, the TL peaks at 134 and 187 ºC are related to phototransfer emissions. Although there are more peaks at high temperatures (i.e., 302 and 460 ºC), they have a very low intensity, so that the phototransfer emission is no longer verified at a temperature above 220 ºC.

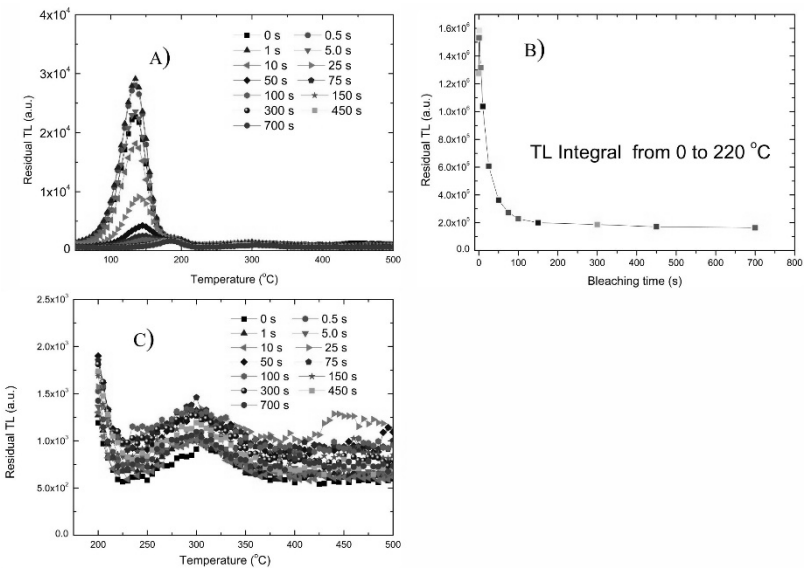

Figure 1.4. A) Residual TL glow curves obtained after bleaching experiments with different blue light time illumination and irradiation with 35.6 Gy. B) The small size plots show the residual TL integral, calculated from 0 to 220 ºC versus bleaching time, C) TL glow curves at the high-temperature region. (After Tudela, 2018).

A large variety of quartz with distinct degrees of impurities is found in the nature, often of different colors, but mostly green, pink, brown and blue. The most abundant in sediments are green and hyaline quartz.

Greater intensity phototransfer emissions were observed in samples with a low concentration of impurities, such as hyaline and pink quartz, and they were absent in green quartz. Trace elements in these two specimens are quite different, with the green quartz containing a large range of impurities, which provide excellent OSL emissions. By contrast, crystals with a few impurities have traps originated predominately from crystalline defects, such as vacancies and lattice distortions, which appear to be less effective in trapping charges (Tudela, 2018).

1.2.4 Determination of equivalent dose - SAR protocol

Wintle and Murray suggested using the SAR protocol (Murray and Wintle, 2000; Wintle and Murray, 2006) to determine the D_e. In this protocol, each aliquot (~ 3 mg) is subjected to repeated preheating and irradiation steps, thus the varying effect on grain sensitivity must be corrected. To correct this variation in crystal grain sensitivity, test doses (D_T) are applied, and measurements are made before determining the regenerative doses used to construct the dose-response curve, even after measurement of the natural signal. The dose used is always constant and generally determined based on the estimated value of D_e, with the following value being adopted: D_T is approximately 10% of D_e (Murray and Wintle, 2000), as required for the effectiveness of the SAR protocol. A general SAR protocol was suggested by Wintle and Murray (2006):

Given dose[a], (D_i)
Preheat (160 - 300 ºC for 10 s)
Stimulate (125 ºC, 40 s) (L_i)
Test dose, D_T
Heat (160-300 ºC)
Stimulate (125 ºC, 40 s) (T_i)
Stimulate (280 ºC, 40 s)
Return to 1
[a] *natural sample, i=0, and $D_{0=}$ natural dose.*
L_i and T_i are obtained from OSL decay curves, typically is the OSL of 1-10 s minus the background from the last part of the OSL decay.

Results of the OSL signal and dose-response curve using the SAR protocol for green quartz is shown in Fig.1.5A, B. The set of D_e values and final D_e value after the application of the SAR protocol can be evaluated after statistical analyses. Thus, age models can be applied according to the historical circumstances of the sediment samples, such as depositional

conditions and past remobilization, which may affect the respective D_e overdispersion results. If the dispersion value of a set of D_e is less than 20%, then the Central Age Model (CAM) (Galbraith et al., 1999, Olley et al., 2004) is applied. If the dispersion is greater than 20%, the Minimum Age Model (MAM) is used, which is generally the case of fluvial sediments or archaeological soils, with sediments exposed to sunlight having high age dispersion. Finite Mixture Model (FMM) is applied in cases where there is a likelihood of finding discrete D_e values, such as in archaeological sites where reoccupation may occur. Aliquots with different D_e values may result in this instance, and the FMM can differentiate these individual temporal components (Galbraith and Roberts, 2012). Age examples obtained with green quartz is shown in Fig.1.5D, F.

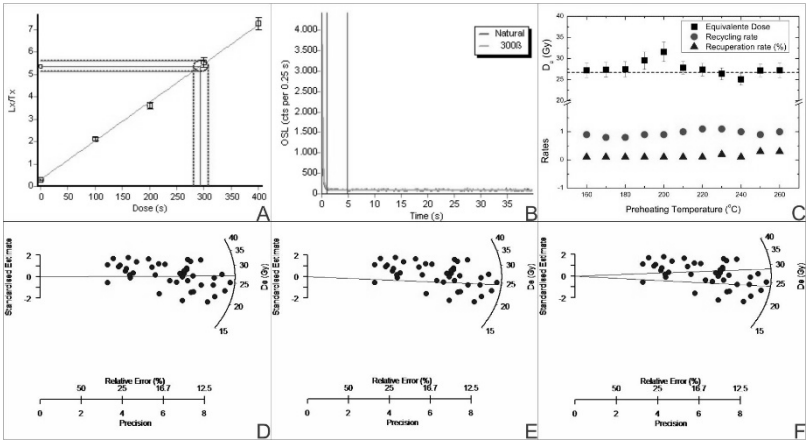

Figure 1.5: A) Example of OSL signals. B) OSL growth curves for green quartz. C) Dose recovery test, a simulated dose of 26.7 Gy at different preheat temperatures, and results of recycling and recuperations ratios. Radial plot for aliquots approved in the recycling and recuperation tests. D) CAM. E) MAM and f) FMM. (After Tudela, 2018).

In addition to the D_e determination, three tests are generally performed to examine the characteristics and physical properties of crystals used in dating. If the crystals pass the tests, the D_e can be considered physically acceptable. The tests are:

1. Dose recovery, performed to observe if the parameters used in the SAR protocol (i.e., heating temperatures and test dose) are effective when adjusted for a specific sample. For this, the OSL signal is initially bleached and subjected to an earlier known dose D_r, and

the SAR protocol is used to recover the D_r dose. If a close value is determined, we can make sure that the parameters used are valid.

2. Recycling test, applied to investigate sensitivity changes during the construction of the OSL dose-response curve, which is the value obtained by the rate $\frac{R_i}{R_1} = \frac{L_1/T_1}{L_i/T_i}$, where L_1 and L_i are measurements after regenerative doses, and T_1 and T_i the OSL after test doses, with this rate being between 0. 9 and 1.1.
3. Recuperation test of OSL signal, related to the intensity emitted without previous irradiation with ionizing radiation (zero doses). Some samples present OSL intensity due to the transfer of charges from deeper traps after irradiation, optical stimulation, and preheating. Results are expressed either as a percentage of the natural signal or as a percentage of the equivalent dose, with the values not exceeding 5% (cf. Murray and Wintle, 2000).

Fig.1.5C shows an example of the results of tests applied to investigate the characteristics and physical properties of green quartz, in which 38 of a total of 43 aliquots passed the recycling and recuperation tests. The same tests were performed on hyaline quartz, which did not pass the tests (Tudela, 2018). SAR protocols were performed at higher preheat temperatures attempting to avoid the phototransfer phenomenon, which suggest that impurities play an important role in the luminescent center stability. However, unusual growth curves were obtained, as well as early saturation of dose-response and some great errors in D_e values. These behaviours are seen in selected quartz sediments commonly used in dating.

The continuous improvements in the OSL dating methodology resulted in the extensive use of samples that have not been burned, which has reached the zero-age by sunlight exposure.

Sedimentary grains used for dating are taken from sites containing natural radioactive isotopes (found in their surrounding area), which, even in small amounts, constantly ionize them. A small part of the energy deposited in these grains is cumulative and proportional to the time (Age) in which the grain was subjected to irradiation. OSL emission occurs if the grain is optically stimulated. The intensity of OSL allows determining the ionization-time of minerals. The "clock", represented by the ionization of the crystals, is known to be zeroed when the grains are exposed to strong heating or solar radiation in the case of TL or OSL, respectively. However, heating can also cause the OSL decay.

It is known that the OSL emitted by quartz and feldspar decays within a few minutes of sunlight exposure, while the TL signal decays to a residual and constant value after a few days of exposure. Therefore, the

use of OSL is most effective in dating unburnt samples. For most samples, the OSL method allows determining ages of Quaternary sediments ranging from a few hundred years to about 1 million years, with uncertainties of up to 10%. Ages greater than 1.5 Ma were documented when using quartz grains from low radiation environments (Huntley et al., 1993a, b). However, the maximum age using the SAR protocol is usually around 100,000 years.

1.2.5 Determination of annual dose rate

As previously mentioned, the OSL of sediments in nature is mainly induced by the exposure to the nuclear radiation emitted by the radioactive elements ^{40}K, ^{232}Th, ^{238}U,^{235}U, and their respective radioactive daughters. Although the contribution of cosmic radiation is generally small, it should be considered when performing OSL dating.

The emission of gamma radiation, as well as of beta and alpha particles, occurs with the disintegration of these radioactive elements. Gamma radiation has higher ionization efficiency and can penetrate to a depth of approximately 30 cm. This kind of radiation corresponds to photons that carry the excess energy from about keV to several MeV, which is generated when the nuclei transition from excited to lower energy states. Beta particles have the energy of a few hundred keV and an average range penetration of 1 to 4 mm. Alpha particles have very little penetration power between 0.01 and 0.05 mm, but high ionization efficiency. The contribution of alpha particles is generally low because HF is usually used to remove the grain surface.

Primary cosmic rays consist predominantly of high energy protons and a mixture of nuclei with very large atomic masses. The average energy is around GeV, and the intensity of its spectrum decreases considerably in the high energy range. Cosmic rays that reach the Earth's surface are divided into two components: low-energy radiation composed mainly of electrons that are absorbed after penetrating 0.5 m into the ground, and high-energy radiation consisting predominantly of muons.

Cosmic rays have a certain dependence on latitude, because the Earth's magnetic field influences the low-energy radiation. There is a variation in the intensity of cosmic rays as a function of the geomagnetic latitude, with the intensity increasing approximately 7% from the Equator to latitudes of 40^{o} and remaining practically constant for higher latitudes (Prescott and Stephan, 1982). The intensity of the cosmic rays may also vary with the altitude of the studied site. Therefore, the contribution of cosmic radiation

can be theoretically calculated by knowing the geological coordinates, altitude, and depths of the sampling sites.

The dose rate in buried sediment can be calculated by determining the concentrations of radioelements in a sediment sample using several methods, such as high-resolution gamma spectroscopy, neutron activation analysis, and inductively coupled plasma mass spectroscopy (ICPMS). However, the absorption coefficients for water are significantly higher and dependent on the type of radiation, which requires a correction using equations 1.4 and 1.5. Gamma, beta, and alpha dose rates can be determined using the conversion table of radionuclide concentration to an effective dose rate (Aitken, 1998).

1.2.6 Results of the OSL dating technique applied to Amazonian sediments

1.2.6.1 Annual dose rates

The two main types of Quaternary sediments in the Amazonian wetlands were formed in fluvial and megafan depositional environments (refer to Chapter 2 for more detailed information about the depositional context). Annual dose rates of samples from fluvial deposits are generally higher compared to the values of these isotopes in samples from megafan deposits. This is illustrated in Tables 1.1 and 1.2, which show several examples of samples from fluvial and megafan deposits with radioactive isotope values ranging from 1.15 to 1.96 Gy/yr and from 0.16 to 1.12 Gy/ky, respectively. In general, the content of natural radioactive isotopes documented for samples in many areas of the Amazonian wetlands is of magnitude lower than approximately 2.0 Gy/ky (Rossetti et.al, 2015, 2017a, 2018a, b, 2019a; Gonçalves Júnior et al., 2016). This is lower than the contents commonly found in fluvial and megafan deposits elsewhere on Earth. For instance, dose rate values range from 1 to 2.04 Gy/ky in fluvial terraces in the upper Hunter catchment in southeastern Australia (Fu et al., 2019), 2.7 to 4.77 Gy/ky in fluvial sediments from the Weihe Basin of central China (He et al., 2019), and 2 to 3 Gy/ky in fluvial terraces of the Yangtze River, also in China (Gao et al., 2019). High dose rates were similarly recorded in sediments from megafans, for instance: 5.39 to 7.55 Gy/ky in sediments of the Upper Ganga Plain megafans, in the central part of the State of Uttar Pradesh in India (Singh et al, 2006); 3.59 to 6.58 Gy/ky in the Tista megafan of the Himalayan proximal foreland (Abrahami, 2018); and 2.24 to 3.30 Gy/ky in the Gwydir megafan of southeastern Australia (Pietsch et.al., 2013). On the other hand,

Quaternary alluvial sediments from interior Oman in southern Arabia provided unusual low dose rate values between 0.17 and 0.77 Gy/ky (Blechschmidt et al., 2009). In this case, the concentration of U and Th was below 1ppm, with some few exceptions, while the concentration of K ranged from 0.05% to 0.18%, the latter resulting in older ages up to 900 kanos (Blechschmidt et al., 2009). Similar low dose rates and old ages have been reported for a sediment sequence from Morocco (Rhodes et al., 2006).

The lower dose rate values recorded in the sediment samples of the Amazonian wetlands compared to those found elsewhere in the globe are related to the low K concentrations. The concentration of this radioactive element in sediments is generally less than 5 %, while in Amazonia is practically negligible (see K values in Tables 1.1 and 1.2). The small amount of K in the Amazonian samples is confirmed by the gamma spectrum emitted by the samples. A gamma spectrum representative of these samples is shown in Fig. 1.6. The concentration of ^{232}Th is evaluated using the 238 and 2614 keV peaks integrals, and the concentration of ^{238}U at 295, 352, 1120 and 1764 keV peaks. The ^{40}K decay counts at 1460 keV are extremely low, which proves the small amount of ^{40}K in the sample.

As an unstable mineral, feldspar grains, when present in this tropical region, are often transformed in clay minerals. Feldspars emit luminescence when excited with infrared light (IRSL), so IRSL measurements generally are performed on selected grain aliquots after chemical etching. Feldspars may also contain high U and Th contents, which increase the annual dose rate values, but the dose rates determined from Amazonian samples are small, ranging from 0.16 to 1.12 Gy/ky. The K concentration is also low, which is due to the lithological composition of sands and sandstones in this region, which consists essentially of quartz grains. Quartz is a very stable mineral that resists transportation, weathering, and diagenesis during burial. Thus, it is the main constituent of the Amazonian sands and sandstones.

Table 1.1: Information about samples of the Madeira River fluvial terraces, including depths, geographic coordinates, radioisotope concentrations, water content (*W*), annual dose rates for the cosmic radiation (AD_{cr}), and total rate values (*AD*).

Sample name	Depth (m)	Coordinates Latitude/longitude	U (ppm)	Th (ppm)	K (%)	*W* (%)	AD_{cr} (μGy/y)	*AD* (Gy/ky)
PV88A1	0.5	7º 32'55'' S/62º 52'38'' W	2.66±0.07	9.50±0.47	0.21±0.01	10	190	1.68±0.03
PV94A1	0.5	7º 35'34'' S/63º 11'23'' W	1.75±0.07	6.46±0.38	0.10±0.01	9	200	1.15±0.03
PV94A2	5.8	7º 35'34'' S/63º 11'23''W	1.80±0.07	6.65±0.39	0.11±0.01	9	84	1.19±0.03
PV94A3	3.0	7º 35'34'' S/63º 11'23'' W	1.89±0.07	7.14±0.42	0.17±0.01	8	123	1.23±0.03
PV101A1	1.8	7º 30'04'' S/63º 24'55'' W	2.73±0.07	14.04±0.70	0.20±0.01	11	150	1.96±0.05
PV111A1	0.4	7⁰ 55'57'' S/63⁰14'04" W	3.27±0.07	7.64±0.40	0.06±0.01	8	193	1.55±0.03
PV120A1	0.9	7º 57'18'' S/63º21'41'' W	1.81±0.07	9.35±0.43	0.08±0.01	9	177	1.49±0.03
PV122A1	1.0	7º 33'43'' S/62º48'45'' W	2.05±0.07	9.31±0.40	0.10±0.01	9	174	1.40±0.03
PV123A1	2.5	7º 17'14'' S/63º09'48'' W	1.82±0.07	11.3±0.46	0.29±0.02	8	134	1.64±0.04

Table 1.2: Information about samples of the Viruá megafan, including depths, geographic coordinates, radioisotope concentrations, water content (*W*), annual dose rates for the cosmic radiation (AD_{cr}), and total rate values (*AD*).

Sample name	Depth (cm)	Coordinate latitude/longitude	U (ppm)	Th (ppm)	K (%)	*W* (%)	AD_{cr} (μGy/y)	*AD* (Gy/ky)
CL3(0.2)	0.2	01° 16' 12.3''N/61°00'56.4''W	2.10±0.10	2.63±0.10	0.05±0.01	9	189	0.92±0.04
CL4(2.9)	2.9	01° 16' 09.4''N/6100'55.7''W	1.92±0.10	4.90±0.20	0.02±0.01	6	118	0.88±0.06
CL4(5.5)	5.5	01° 16' 09.4''N/6100'55.7''W	1.94±0.10	4.30 ±0.20	0.01±0.01	5	78	0.82±0.05
CL6(0.5)	0.5	01° 16' 14.1''N/6100'54.8''W	1.33±0.07	1.03±0.05	0.05±0.02	8	179	0.68±0.34
CL6(5.5)	5.5	01° 16' 14.1''N/61°00'54.8''W	1.82±0.09	6.29±0.25	0.07±0.01	6	78	0.95±0.02
CL13(0.4)	0.4	01° 11' 59.7''N/61°07'39.6''W	0.51±0.09	0.20±0.01	b.d.l.	7	182	0.30±0.02
C14(0.3)	0.3	01° 15' 04.5"N/61° 06'21.1''W	0.76±0.10	0.30±0.01	b.d.l	8	185	0.37±0.02
CL14(2.3)	2.3	01° 15' 04.5"N/61° 06'21.1''W	1.44±0.10	2.70±0.01	b.d.l	7	130	0.64±0.04
CL15(0.3)	0.3	01° 21' 18.3"N/60° 58'55.5''W	1.68±0.08	1.74±0.09	0.06±0.01	10	185	0.81±0.03

CL15(1.7)	1.7	01° 21' 18.3"N/60° 58'55.5''W	2.58±0.12	4.49±0.17	0.06±0.01	8	144	1.08±0.03
CL15(3.5)	3.5	01° 21' 18.3"N/60° 58'55.5''W	2.44±0.11	5.96±0.23	0.06±0.01	7	107	1.07±0.03
CL15(4.9)	4.9	01° 21' 18.3"N/60° 58'55.5''W	0.97±0.05	2.18±0.29	0.05±0.01	6	86	0.79±0.02
CL16(0.7)	0.7	01° 21' 15.7"N/60° 58'54.0''W	2.20±0.11	3.00±0.23	0.06±0.01	10	172	0.90±0.03
CL20(1.1)	1.1	01° 16' 20.3"N/60° 58'09.7''W	2.25±0.11	3.50±0.20	0.02±0.01	6	160	0.16±0.01
CL21(0.5)	0.5	01° 16' 22.5"N/60° 58'10.2''W	2.45±0.12	4.53±0.18	0.06±0.01	12	179	1.01±0.04
CL25(1.1)	1.1	01° 16' 52.8"N/60° 59'46.5''W	2.24±0.11	5.75±0.23	0.06±0.01	7	160	1.12±0.03
CL27(1.9)	1.9	01° 18' 07.4"N/60° 58'30.8''W	1.44±0.09	1.30±0.20	0.02±0.01	5	139	0.54±0.03

b.d.l.= Below detection limit

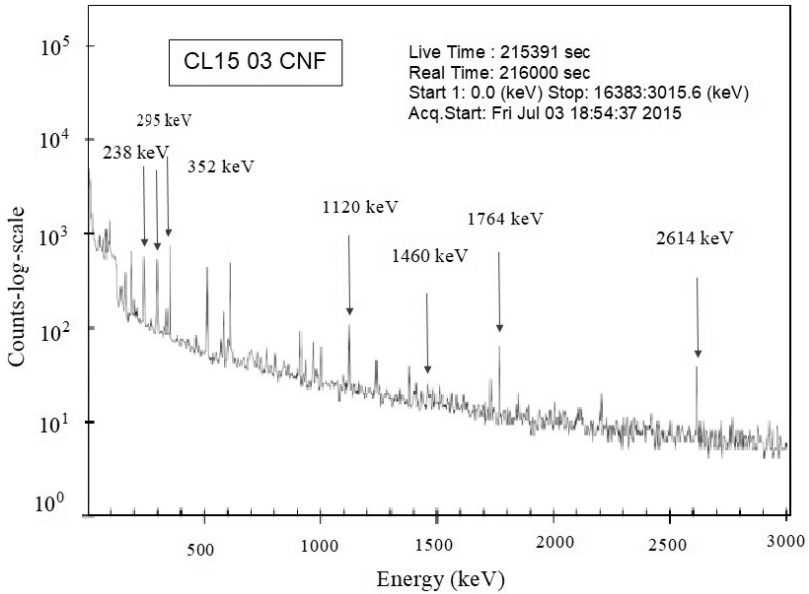

Figure 1.6: Example of gamma spectrum of a sediment sample from the Amazonian wetlands obtained with HPGe.

1.2.6.2. Water content

The water contents of the samples were measured for the OSL dating of Amazonian sediments. This parameter was used to make final corrections, since the sediments were mostly deposited in subaqueous environments, but are no longer submerged. Interstitial water in the grains can absorb some of the radiation, thus only a proportion of the radiation emitted by the natural radioisotopes is absorbed by the grains. Theoretical calculations can compensate for this effect, but an estimation of the water content over the burial period is required. Although this parameter is difficult to be estimated, some constraints can be considered. For example, the upper limit can be determined by measuring the saturation of the modern-day water content. The influence of water on the dose rate varies from sample to sample, and this is a source of uncertainty when estimating the final age of the sediments. This is particularly troublesome when dating subaqueous alluvial deposits, and specific attenuation factors need to be used in dose rate calculations. Usually, when the water concentration

increases by 1%, the age also increases by about 1%. In the case of the samples studied, the average moisture was about 8 % (Table 1.1 and 1.2).

1.2.6.3. Measurement technique of radioisotope contents

High-resolution gamma spectroscopy using a high purity germanium detector (HPGe) and an ultra-low background shield from the Canberra Industry was adopted to date sediment samples of the Amazonian wetlands. The sample spectra were compared to those emitted by the soil standard samples JR-1, JB-3, JG1a, and JG-3. The Adamiec and Aitken (1998) conversion table was used to evaluate dose rates. To use this conversion table, the condition of secular equilibrium must be attained, where the decay rate of each daughter is the same as the parents in the Th and U decays. The radioactive disequilibrium can generally occur with an escape of gaseous daughter radon. To establish the secular equilibrium, the samples were placed in the sample holders and sealed for two weeks before the measurement. The cosmic radiations were theoretically calculated with the equations of Prescott and Hutton (1994).